Dynamic Oxidation of $(Mn,Co)_3O_4$-Coated Interconnects for Solid Oxide Electrolysis Cells

Fengyu Shen[1], Sergio A. Ibanez[2], Michael C. Tucker[1*]

1. Energy Conversion Group, Lawrence Berkeley National Laboratory, Berkeley, CA 94720
2. Nexceris, Lewis Center, OH 43035

Abstract

Solid oxide electrolysis cell stacks are expected to experience dynamic conditions when using renewable electricity derived from wind or solar power. To address this scenario, $(Mn,Co)_3O_4$ (MCO)-coated Crofer 22 APU interconnect coupons are subjected to thermal cycling, and intermittent current density, with gas compositions relevant to high-temperature electrolysis (elevated steam:hydrogen ratio and oxygen content). Defects are also intentionally introduced in the MCO coating, to assess whether the difference in oxidation properties of the adjacent coated and uncoated (defective) surfaces causes sufficient stress to damage the protective oxide scale. Specimens with defects are subjected to oxidation for 1000 h at 800°C, or thermal cycling. Before thermal cycling, some specimens are pre-oxidized to create a thick oxide scale to mimic the scale thickness expected after ~30 kh operation. In all cases, the coating and oxide scale remain well adhered with no cracking observed. Area-specific resistance (ASR) is monitored in both single-atmosphere and dual-atmosphere conditions, and the ASR is stable and is not impacted by dynamic cycling of the current density. This work provides confidence that the MCO coated interconnect will function as needed in dynamic operation conditions, even with coating defects.

Keywords: SOEC; electrolysis; oxidation; stainless steel; interconnect; coating

Introduction

Solid oxide electrolysis cells (SOECs) produce hydrogen from inputs of electric power, steam, and possibly waste heat. Ideally, the SOEC high-temperature electrolyzer (HTE) system can accept dynamic or intermittent sources of electric power, such as wind or solar. In such cases, the SOEC cell stacks experience wide and rapid variation in key operating variables including temperature, voltage, current density, steam utilization, etc. [1, 2]. This can exert stresses on all components of the stack, including the interconnects, seals, and SOEC cells.

Interconnects are a key component of the electrolyzer stack, and their development has been extensively reviewed [3-5]. They provide electrical connection between adjacent cells, while separating the steam-side and oxygen-side gas streams. Interconnects are typically made from ferritic stainless steel, and cut or stamped to create flow channels. The oxygen-side of the interconnect is coated to reduce the rates of Cr evaporation and oxidation. A Cr_2O_3-based scale forms on the surface of the stainless steel, adjacent to the coating. This scale is protective, leading to parabolic growth rate kinetics that support an acceptable lifetime. The scale is, however, more resistive than the bulk stainless steel. Therefore, as the scale thickness grows during operation, the area-specific resistance (ASR) increases with time, leading to electrolyzer performance degradation. The performance and integrity of the interconnect and its coating are therefore critical for viability of the HTE technology.

Interconnect oxidation studies in the literature typically report scale thickness of ~1 μm after 1000 h or less, with a few reports as long as 3 to 5kh [6, 7]. While this timeframe is useful for assessing initial oxidation rate, it does not offer any insight into the risk of spallation near the end of stack lifetime, when the Cr_2O_3 scale is expected to be quite thick. For example, the calculated scale

thickness is 6 or 10 μm after 30 or 70 kh of operation for an oxidation rate of 10^{-14} $g^2cm^{-4}s^{-1}$, which is a typical rate for coated ferritic stainless steel at 800°C [8-10]. For such thick scales, it is a concern that thermal cycling may cause the protective chromia scale to spall or flake off of the stainless steel substrate due to coefficient of thermal expansion (CTE) mismatch (~11 ppm/K for ferritic stainless steel and ~7 ppm/K for Cr_2O_3). That risk is evaluated here, by producing interconnect coupons with a range of scale thickness up to ~6 μm, and subjecting them to extended thermal cycling. Although there are some reports of interconnect oxidation during initial thermal cycling [11, 12], we are not aware of any that demonstrate it with thick chromia scales.

Scratches, pinholes, residual porosity, and other defects in the coating may similarly present a concern due to stress associated with widely varying scale growth in the vicinity of the defect. The uncoated area under the defect is expected to have an oxidation rate up to 10 times higher than the coated area [8, 9, 13], resulting in a scale thickness about 4 times thicker [10]. Here, defects are intentionally introduced into the coating, revealing bare stainless steel. These samples are subjected to extensive oxidation and thermal cycling to determine if the scale thickness variation is indeed an issue for scale integrity. Although there are reports of defects in the scale and defect chemistry of the coating [14, 15], we are not aware of any that address macroscopic defects in the coating.

In addition to thermal cycling, electrolyzers utilizing dynamic or intermittent renewable electricity must tolerate variability in the electric load. There are many reports of SOEC cells and stacks responding to cyclic loads [16-18], but cycling of the interconnect alone is lacking. Here, dynamic power loading of the interconnect and coating is represented by cycling the current density while monitoring the ASR in both single-atmosphere and dual-atmosphere configurations.

The ChromLok^{TM} $(Mn,Co)_3O_4$ (MCO)-based coating produced by Nexceris is designed for stainless steel interconnects. Previously, viability of the Chromelok coating for stable SOEC conditions was demonstrated via galvanostatic operation of a stack for 700 h isothermally at 800°C [8]. In ex-situ isothermal evaluations, the coating was found to dramatically reduce oxidation, Cr evaporation, and ASR degradation. That effort is continued here, by evaluating the impact of more realistic operating conditions, including thermal cycling, the presence of coating defects, and dynamic power loading.

Experimental

Sample preparation

Crofer 22 APU stainless steel sheets (0.3 mm thickness) were cut into 2 x 2 cm coupons. For coated samples, ChromLok^{TM} $(Mn,Co)_3O_4$ (MCO) powder was synthesized, milled to produce 8 to 10 $m^2\ g^{-1}$ surface area, and incorporated into a suspension for coating. Coupons were coated with MCO using aerosol spray deposition. The coupons were then heat treated in reducing atmosphere and air to form a ~12 μm thick MCO coating, similar to previous studies [19-21]. These as-received (AR) samples contain a ~1 μm thick chromia scale at the surface of the stainless steel [8].

Defects were introduced into the continuous coating by laser ablation. A fiber laser cutter (Full Spectrum Laser) was used to cut through the coating, revealing the metal substrate below. The laser path was about 90 μm total width, with about 60 μm focused cutting width. Various cut depths were achieved by varying the number of passes, Figure S1. The power was held at 30%, the scan rate was 200 cm s^{-1}, and the pulse rate was 80 kHz.

Oxidation

Coated and pristine uncoated coupons were oxidized in ambient air at 1000°C to produce a ~6 μm thick chromia scale. The time required to achieve this thickness was determined to be 150h for coated coupons and 20 h for uncoated coupons, which resulted in similar weight gain during this preoxidation, Table 1. The coupons were then subjected to cyclic thermal oxidation in a tube furnace with alumina tube and flowing "oxygen-side" (30% O_2/3% H_2O/67% N_2) or "steam-side" (75:25 H_2O:H_2, 2.8% H_2/8.4% H_2O/88.8% Ar) atmospheres. The humidity was controlled by flowing the gases through a temperature-controlled water bubbler. The coupons were cycled 200 times between 70 and 800°C, with 7°C/min heating rate, 4°C/min average cooling rate, and 1 h hold at 800°C. Samples with coating defects were oxidized continuously in oxygen-side atmosphere for 1000 h at 800°C, or subjected to the same thermal cycling as above. Additionally, some defect samples were oxidized for 150 h at 1000°C before thermal cycling.

ASR

Coupons for ASR testing were prepared by attaching Pt mesh current and voltage leads to both sides. For single atmosphere testing, and for the oxygen side of dual atmosphere testing, a 1 cm^2 square active area was defined by applying Pt paste (Heraeus CL115349), followed by Pt mesh (Johnson Matthey, 52 mesh), and firing at 1000°C in air for 1 h. For dual-atmosphere testing, Pt mesh was spot welded onto the steam side before adding Pt paste. This created a strong and very low-resistance connection on the steam side, so as to isolate the performance of the coating on the oxygen side. For ASR testing, the Pt meshes were spot welded to Pt wires for voltage sensing and current. Current was applied by an electronic power supply (GW Instek GPR-1810HD), and

voltage was monitored with a data acquisition unit (Madgetech Volt101A). ASR coupons were held at 800°C in tube furnaces with 30% O_2/3% H_2O/67% N_2 for single atmosphere testing, or 30% O_2/3% H_2O/67% N_2 and 75:25 H_2O:H_2 (2% H_2/6% H_2O/92% Ar) for dual-atmosphere testing. The dual atmosphere test rig was a conventional SOFC button cell alumina tube test rig with heated inlet gas lines as described in detail elsewhere [22], with the coupon sealed and bonded with Ag paste fired at 800°C. Details of the seal selection and test rig development are available in the Supplementary Information. Various current protocols were used. "Constant" was 2 A cm^{-2} galvanostatic current. "No current" had 2 A cm^{-2} passed for only 10 min each day to monitor ASR evolution. "Cycling" switched between no current and 2 A cm^{-2} with holds of 2 h (single atmosphere) or 1 h (dual atmosphere).

Characterization

After oxidation, surface morphologies and cross-sections of epoxy-mounted samples were observed by scanning electron microscopy (SEM) using a Zeiss Gemini Ultra-55 FESEM with an energy dispersive x-ray spectrometer (EDS).

Results and Discussion

MCO-coated stainless steel samples are subjected to thermal cycling, with and without defects in the coating. The impact of dynamic current is then assessed by comparing constant current and cycled current in both single- and dual-atmosphere configurations. Post-mortem analysis with SEM/EDS is used to assess the impact of these dynamic operating conditions on the scale and coating integrity.

1. Thermal cycling of continuous coatings

The impact of thermal cycling on specimens with minimal, thin, or thick protective chromia scales was determined in oxygen-side and steam-side atmospheres. The risk of spallation is higher for thicker chromia scales, which develop after long-term operation (10's of kh). To represent the scale thickness after long-term operation, thick scales were fabricated by pre-oxidation to generate a target thickness of ~ 6 μm. For comparison, samples with a thin scale were prepared by oxidizing in air at 1000°C for 1 h. Note that the as-received (AR) coated samples had a thin ~1 μm scale produced during coating fabrication [8].

Table 1. Thermal cycling results.

Atmosphere, coating	Oxygen side, coated			Oxygen side, un-coated			Steam side, un-coated		
Cr_2O_3 scale	AR	Thin	Thick	AR	Thin	Thick	AR	Thin	Thick
Scale preparation weight gain (mg cm^{-2})	-	0.04	1.04	-	0.18	0.87	-	0.19	0.83
Thermal cycling weight gain (mg cm^{-2})	0.01	0.02	0.01	0.13	0.03	0.02	0.24	0.10	0.06

A total of 200 thermal cycles (70 to 800°C) were accumulated with no sign of spallation. The weight gain after thermal cycling was quite low for samples that were coated or preoxidized, Table 1. The uncoated samples oxidized significantly in both oxygen-side and steam-side atmospheres. The weight gain during scale preparation was dramatically higher than the weight gain during subsequent thermal cycling, consistent with the prepared scale being protective against further oxidation. Post-cycling SEM analysis determined that the MCO coating and Cr-scale were uniformly well bonded to the Crofer substrates after thermal cycling, with no delamination, spallation, or cracking observed for all samples. Representative SEM/EDS analysis for thick pre-oxidation scales cycled in both atmospheres are shown in Figure 1. The scale thickness after

preoxidation and thermal cycling was in the range 5 to 7 μm. Note that this is much thicker than the ~1 μm scales observed for typical short-term interconnect oxidation studies reported in the literature [6], and as such this offers valuable evidence that MCO-coated Crofer interconnects will survive without scale damage during long-term operation. These results suggest that scale failure due to thermal cycling is unlikely, even after long-term oxidation during operation, at least at the typical temperature ramp rates studied here.

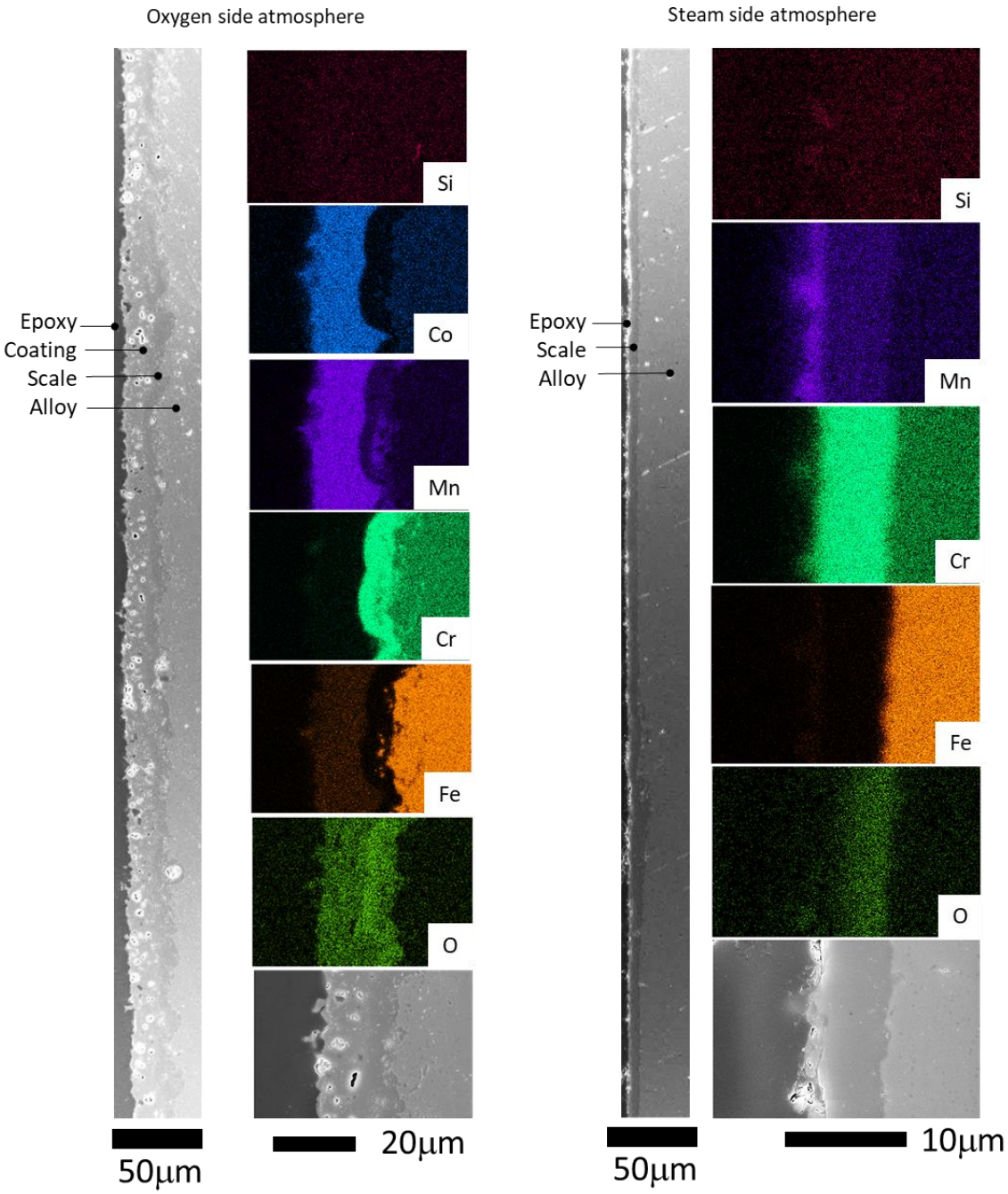

Figure 1. Thermal cycling. Polished cross-section SEM/EDS images of surface layers after 200 thermal cycles from 70 to 800°C. (Left) MCO-coated stainless steel cycled in oxygen-side atmosphere. (Right) Uncoated stainless steel cycled in steam-side atmosphere. Both samples were pre-oxidized at 1000°C to

produce a thick scale before thermal cycling. Note that the magnification for the element mapping is different for the two samples.

2. Oxidation and thermal cycling of coatings with defects

Defects in the MCO coating were introduced by laser cutting, Figures 2 and S1. The cut width was around 60 μm and the depth of cut was adjusted by the number of laser cutting passes. The desired result is removal of the MCO coating with minimal removal of the underlying metal, which was achieved for 10 to 30 laser passes. Samples with defects were subjected to long-term oxidation (1000 h at 800°C) or 200 thermal cycles in oxygen-side atmosphere. As above in Section 1, some samples were pre-oxidized to create a thick scale before thermal cycling, to exacerbate thermal stress. After 1000 h oxidation, no cracks or delamination were observed, Figure 3. Co was absent from the center of the laser cut, indicating complete removal of the coating. There is a continuous protective scale, composed of Cr-oxide and (Cr,Mn)-oxide. There is some Fe-rich oxide in the center of the cut, suggesting some localized breakaway oxidation occurred. This is not expected to be an issue for long-term durability, as the remaining coating near the defect continues to provide oxidation protection. SEM/EDS linescans (Figure S2) show that the oxide scale is 4.5 μm thick under the coating, and 7 to 9 μm thick in the defect area. Any stress caused by the mismatched scale growth rate is not sufficient to damage the scale or coating. Additional thermal stress from thermal cycling also did not cause cracking or delamination, Figure 4. Both thin (no preoxidation) and thick (preoxidized 150h at 1000°C) oxide scales are continuous and well-adhered to the alloy and MCO coating after 200 thermal cycles. Some Cr is observed on the edges of the coating, and this is thought to originate from alloy ejection from the laser during defect cutting. It appears that the Cr remains on the surface near the defect, whereas Fe migrates into the coating.

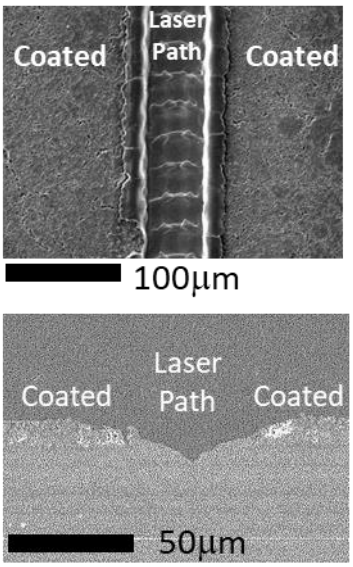

Figure 2. Laser-etched defect. (Top) Top-surface and (bottom) cross-section SEM images of a MCO-coated specimen after laser-etching a defect line into the surface. The laser cut through the MCO coating and produced a shallow trench in the underlying alloy. Laser pulses are visible in the trench.

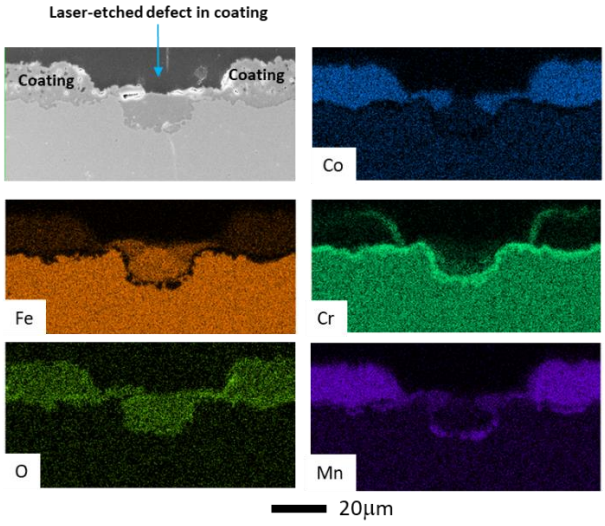

Figure 3. Coating defect after long-term oxidation. Polished cross-section SEM/EDS images of surface layers of an MCO-coated specimen with laser-etched defect, after 1000 h oxidation in oxygen-side atmosphere at 800°C.

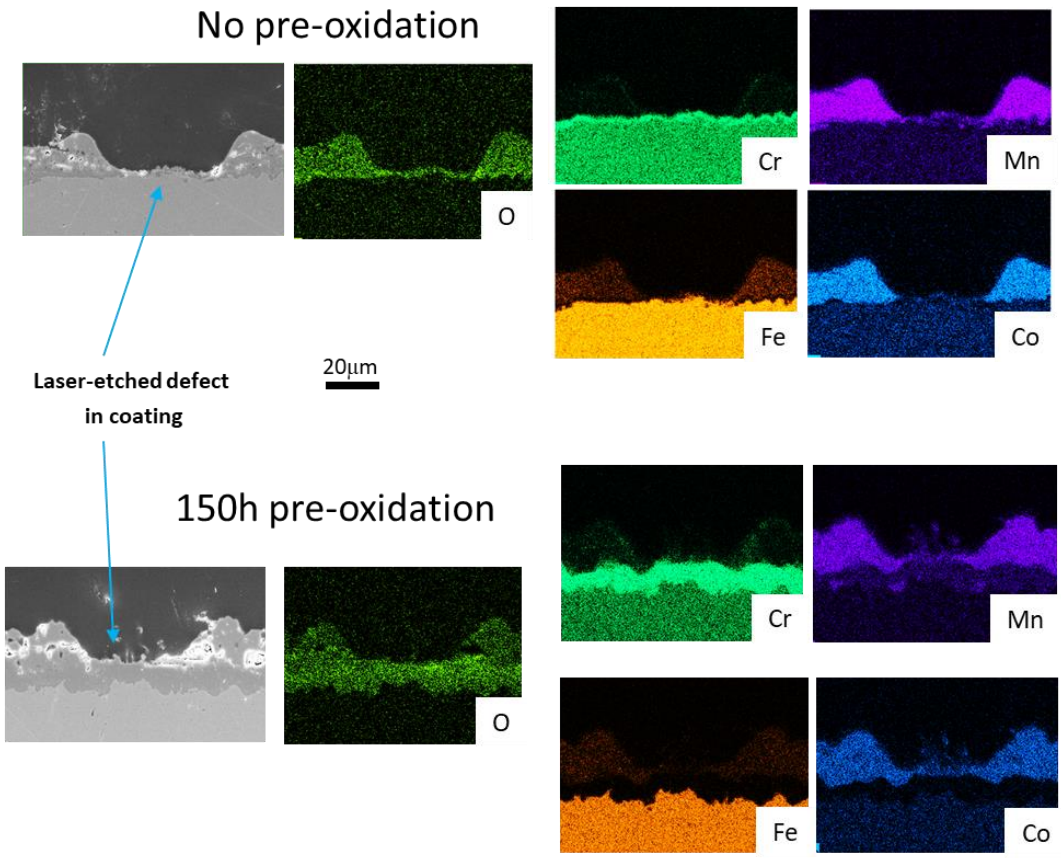

Figure 4. Coating defect after thermal cycling. Polished cross-section SEM/EDS images of surface layers of an MCO-coated specimen with laser-etched defect, after 200 thermal cycles from 70 to 800°C in oxygen-side atmosphere. (Top) Specimen with no oxidation before thermal cycling. (Bottom) Specimen that was pre-oxidized for 150 h in air at 1000°C before thermal cycling.

3. Oxidation with dynamic current load

The interconnect and coating ASR is not impacted significantly by the application of continuous or intermittent current, Figure 5. Current was cycled between 0 and 2 A cm^{-2}, with 2 h holds at each current density. A total of 125 cycles was accumulated. Baseline samples with constant

current density of 2 A cm^{-2} or no current (except for 10 min per day at 2 A cm^{-2} to evaluate the ASR) were also tested. The initial ASR for the three samples varied between 5 and 7 mOhms cm^2 (see Figure S3). This sample-to-sample variation as removed by normalizing to the initial ASR to make a clear comparison of the ASR evolution, Figure 5. The ASR evolution was nearly identical for all samples, suggesting that current cycling does not impact the durability of the coating, accelerate oxidation, or otherwise impact the protective effect of the coating. After an initial transient during the first 200 h, slow continuous degradation of the ASR is observed at 1 mOhm cm^{-2} kh^{-1}, consistent with the ASR degradation of this coating reported previously [8].

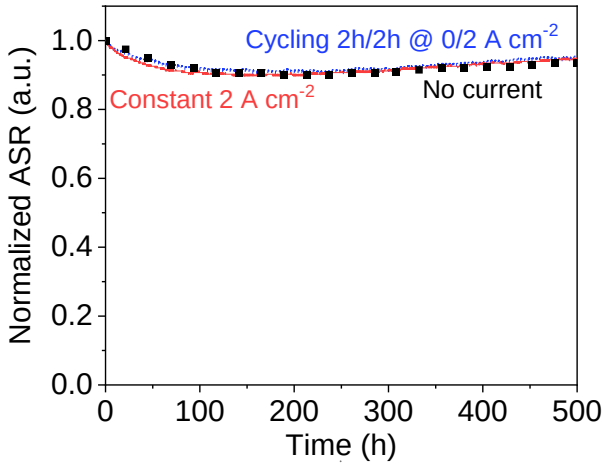

Figure 5. Current cycling. ASR normalized to the initial ASR, for double-side-coated coupons in oxygen-side atmosphere at 800°C with no current (black squares), constant 2 A cm^{-2} (red line), or cycling between 2 h holds at 0 or 2 A cm^{-2} (blue line).

Dual-atmosphere testing was undertaken to more closely mimic the environment of an interconnect in an operating stack, Figure 6. A coupon was exposed to oxygen-side and steam-side atmospheres simultaneously, with coating on the oxygen side only and a bare steam side. The

current was cycled for 500 h between 0 and 2 A cm^{-2}, with 1 h holds. The ASR evolution was very similar to a baseline dual-atmosphere test in which the current was held at 2 A cm^{-2} continuously. Normal oxidation is observed after the dual-atmosphere ASR testing, Figures S5 and S6. At the operating temperature of 800°C used here, protective oxidation is expected in dual atmosphere. In contrast, breakaway and anomalous oxidation in dual atmospheres has been observed at 600°C [23, 24]. Furthermore, the bare stainless steel on the steam side was preoxidized in air during firing of the Pt paste current collector. Preoxidation is known to prevent formation of non-protective iron oxides in steam-side atmosphere [25], and reduce hydrogen transport in dual atmosphere configuration, as diffusion through the oxide scale limits the hydrogen flux [26, 27]. On the oxygen side, the presence of elevated oxygen concentration (relative to air) is not expected to alter the oxidation rate, as the rate was found to be roughly independent of oxygen concentration [28]. SEM observations of the scales after dual atmosphere exposure are consistent with these expectations. Thin, dense, and continuous Cr-oxide and (Cr,Mn)-oxide scale is formed in both the regions with and without current (under the Pt electrode, and away from the Pt electrode), Figures S5 and S6. The results presented in this section increase confidence that the coated interconnect will provide low, stable ASR during dynamic current operation in contact with oxidizing and reducing atmospheres.

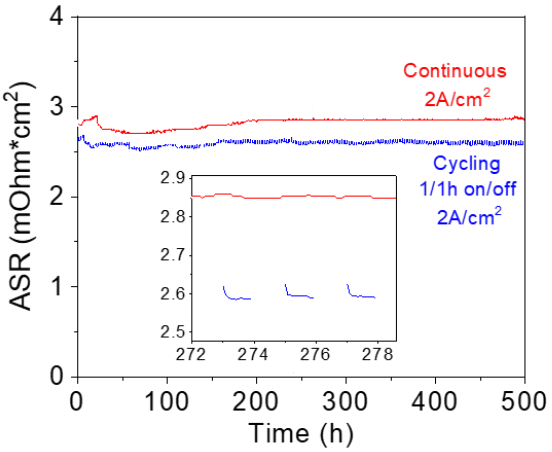

Figure 5. Dual atmosphere ASR. Single-side-coated coupons simultaneously exposed to both oxygen-side atmosphere (coated side) and steam atmosphere (uncoated side) at 800°C with continuous current density of 2 A cm^{-2} (red line), or cycling between 1 h holds at 0 or 2 A cm^{-2} (blue line).

Conclusions

MCO is an effective coating for suppressing the oxidation rate of ferritic stainless steel interconnects. The coating and underlying oxide scale remain well-adhered and continuous with no cracks after 200 thermal cycles. This is the case even when the thermal stress is enhanced by pre-oxidizing the interconnect, thereby introducing a thick oxide scale before thermal cycling. Defects in the coating are well tolerated. A laser cutter was use to mimic a ~60 μm wide scratch defect in the coating. The oxide scale grows more rapidly in the defect area, but the coating and scale remain well-adhered and do not crack after 1000h oxidation, or 200 thermal cycles. In single-atmosphere and dual-atmosphere configurations, the ASR is stable and is not impacted by dynamic

cycling of the current density. This work provides confidence that the MCO coated interconnect will function as needed in dynamic operation conditions, even with coating defects.

Acknowledgements

The authors gratefully acknowledge research support from the HydroGEN Advanced Water Splitting Materials Consortium, established as part of the Energy Materials Network under the U.S. Department of Energy, Office of Energy Efficiency and Renewable Energy, Fuel Cell Technologies Office, under Contract Numbers DE-AC02-05CH11231 and DE-EE0008834. The use of Zeiss Gemini Ultra-55 FESEM in the Molecular Foundry of Lawrence Berkeley National Laboratory was supported by the Office of Science, Office of Basic Energy Sciences, of the U.S. Department of Energy under Contract No. DE-AC02-05CH11231. This work was funded in part by the U.S. Department of Energy under contract no. DE-AC02-05CH11231. Dr. Boxun Hu assisted with initial SEM analysis. The views and opinions of the authors expressed herein do not necessarily state or reflect those of the United States Government or any agency thereof. Neither the United States Government nor any agency thereof, nor any of their employees, makes any warranty, expressed or implied, or assumes any legal liability or responsibility for the accuracy, completeness, or usefulness of any information, apparatus, product, or process disclosed, or represents that its use would not infringe privately owned rights.

References

[1] Hauch A, Küngas R, Blennow P, Hansen AB, Hansen JB, Mathiesen BV, et al. Recent advances in solid oxide cell technology for electrolysis. Science. 2020;370:eaba6118.
[2] Mermelstein J, Posdziech O. Development and Demonstration of a Novel Reversible SOFC System for Utility and Micro Grid Energy Storage. Fuel Cells. 2017;17:562-70.
[3] Chevalier S, Combemale L, Popa I, Chandra-Ambhorn S, Chandra-Ambhorn W, Promdirek P, et al. CHAPTER 6 Development of SOFC Interconnect Stainless Steels. Solid State Phenomena. 2020;300:135-56.
[4] Mah JCW, Muchtar A, Somalu MR, Ghazali MJ. Metallic interconnects for solid oxide fuel cell: A review on protective coating and deposition techniques. International Journal of Hydrogen Energy. 2017;42:9219-29.
[5] Wu J, Liu X. Recent Development of SOFC Metallic Interconnect. Journal of Materials Science & Technology. 2010;26:293-305.
[6] Jia C, Wang Y, Molin S, Zhang Y, Chen M, Han M. High temperature oxidation behavior of SUS430 SOFC interconnects with Mn-Co spinel coating in air. Journal of Alloys and Compounds. 2019;787:1327-35.
[7] Reddy MJ, Chausson TE, Svensson JE, Froitzheim J. 11–23% Cr steels for solid oxide fuel cell interconnect applications at 800 °C – How the coating determines oxidation kinetics. International Journal of Hydrogen Energy. 2023;48:12893-904.
[8] Dogdibegovic E, Ibanez S, Wallace A, Kopechek D, Arkenberg G, Swartz S, et al. Performance of stainless steel interconnects with (Mn,Co)3O4-Based coating for solid oxide electrolysis. International Journal of Hydrogen Energy. 2022;47:24279-86.
[9] Talic B, Falk-Windisch H, Venkatachalam V, Hendriksen PV, Wiik K, Lein HL. Effect of coating density on oxidation resistance and Cr vaporization from solid oxide fuel cell interconnects. Journal of Power Sources. 2017;354:57-67.
[10] Tucker MC. Durability of symmetric-structured metal-supported solid oxide fuel cells. Journal of Power Sources. 2017;369:6-12.
[11] Wu J, Gemmen RS, Manivannan A, Liu X. Investigation of Mn/Co coated T441 alloy as SOFC interconnect by on-cell tests. International Journal of Hydrogen Energy. 2011;36:4525-9.
[12] Yang Z, Xia G, Simner SP, Stevenson JW. Thermal Growth and Performance of Manganese Cobaltite Spinel Protection Layers on Ferritic Stainless Steel SOFC Interconnects. Journal of The Electrochemical Society. 2005;152:A1896.
[13] Molin S, Chen M, Bentzen JJ, Hendriksen PV. High Temperature Oxidation of Ferritic Steels for Solid Oxide Electrolysis Stacks. ECS Transactions. 2013;50:11.
[14] Gannon P, Amendola R. High-Temperature, Dual-Atmosphere Corrosion of Solid-Oxide Fuel Cell Interconnects. JOM. 2012;64:1470-6.
[15] Yun DW, Seo HS, Jun JH, Lee JM, Kim KY. Molybdenum effect on oxidation resistance and electric conduction of ferritic stainless steel for SOFC interconnect. International Journal of Hydrogen Energy. 2012;37:10328-36.
[16] Graves C, Ebbesen SD, Jensen SH, Simonsen SB, Mogensen MB. Eliminating degradation in solid oxide electrochemical cells by reversible operation. Nature Materials. 2015;14:239-44.
[17] Léon A, Micero A, Ludwig B, Brisse A. Effect of scaling-up on the performance and degradation of long-term operated electrolyte supported solid oxide cell, stack and module in electrolysis mode. Journal of Power Sources. 2021;510:230346.
[18] Schefold J, Brisse A, Surrey A, Walter C. 80,000 current on/off cycles in a one year long steam electrolysis test with a solid oxide cell. International Journal of Hydrogen Energy. 2020;45:5143-54.

[19] Abdoli H, Molin S, Farnoush H. Effect of interconnect coating procedure on solid oxide fuel cell performance. Materials Letters. 2020;259:126898.
[20] Hu Y-Z, Yao S-W, Li C-X, Li C-J, Zhang S-L. Influence of pre-reduction on microstructure homogeneity and electrical properties of APS Mn1.5Co1.5O4 coatings for SOFC interconnects. International Journal of Hydrogen Energy. 2017;42:27241-53.
[21] Park B-K, Lee J-W, Lee S-B, Lim T-H, Park S-J, Park C-O, et al. Cu- and Ni-doped Mn1.5Co1.5O4 spinel coatings on metallic interconnects for solid oxide fuel cells. International Journal of Hydrogen Energy. 2013;38:12043-50.
[22] Shen F, Welander MM, Tucker MC. Metal-Supported Solid Oxide Electrolysis Cell Test Standard Operating Procedure. Frontiers in Energy Research. 2022;10.
[23] Alnegren P, Sattari M, Svensson J-E, Froitzheim J. Severe dual atmosphere effect at 600 °C for stainless steel 441. Journal of Power Sources. 2016;301:170-8.
[24] Alnegren P, Sattari M, Svensson J-E, Froitzheim J. Temperature dependence of corrosion of ferritic stainless steel in dual atmosphere at 600–800 °C. Journal of Power Sources. 2018;392:129-38.
[25] Ardigo-Besnard MR, Popa I, Chevalier S. Impact of pre-oxidation on the reactivity and conductivity in H2–H2O atmosphere of a ferritic stainless steel for high temperature water vapour electrolysis. International Journal of Hydrogen Energy. 2022;47:23508-13.
[26] Goebel C, Alnegren P, Faust R, Svensson J-E, Froitzheim J. The effect of pre-oxidation parameters on the corrosion behavior of AISI 441 in dual atmosphere. International Journal of Hydrogen Energy. 2018;43:14665-74.
[27] Skilbred AWB, Haugsrud R. Sandvik Sanergy HT – A potential interconnect material for LaNbO4-based proton ceramic fuel cells. Journal of Power Sources. 2012;206:70-6.
[28] Alnegren P, Sattari M, Froitzheim J, Svensson JE. Degradation of ferritic stainless steels under conditions used for solid oxide fuel cells and electrolyzers at varying oxygen pressures. Corrosion Science. 2016;110:200-12.